Reservoir Stress Path Characterization and its Implications for Fluid-Flow Production Simulations

J.M. Segura[1,2], Q.J. Fisher[1], A.J.L. Crook[2], M. Dutko[2], J. Yu[2], S Skachkov[1], D.A. Angus[1,3], J. Verdon[3], M. Kendall[3]
UNIVERSITY OF LEEDS
ROCKFIELD SOFTWARE LTD
UNIVERSITY OF BRISTOL

Correspondence to: Quentin Fisher, CIPEG, University of Leeds LS2 9JT, q.j.fisher@ leeds.ac.uk

ABSTRACT

The reduction of fluid pressure during reservoir production promotes changes in the effective and total stress distribution within the reservoir and the surrounding strata. This stress evolution is responsible for many problems encountered during production (e.g. fault reactivation, casing deformation). This work presents the results of an extensive series of 3D numerical hydro-mechanical coupled analyses that study the influence of reservoir geometry and material properties on the reservoir stress path. The stress path is defined in terms of parameters that quantify the amount of stress arching and stress anisotropy that occur during reservoir production. The coupled simulations are run using an explicit coupling code between Elfen (Rockfield Software Ltd) and Tempest (Roxar). It is shown that the stress arching effect is important in small or thin reservoirs that are soft compared to the bounding material. In such cases, the stresses will not significantly evolve in the reservoir, and stress evolution occurs in the over and side-burden. Stiff reservoirs do not show stress arching regardless of the geometry. Stress anisotropy reduces with the bounding material Young's modulus, especially for small reservoirs, but as the reservoir extends in one or the two horizontal directions, the reservoir deforms uniaxially and the horizontal stress evolution is governed by the reservoir Poisson's ratio. Furthermore, the effect of the stress path parameters is introduced in the calculation of pore volume multiplier tables to improve non-coupled simulations, which otherwise overestimate the average reservoir pore pressure drawdown when stress arching is taking place.

Keywords: hydro-mechanical coupling, stress path, stress arching

1. INTRODUCTION

Change in reservoir pore pressure due to hydrocarbon production promotes changes not only in the effective stress, but also in the total stress distribution acting on the reservoir and the surrounding rock. If the total stres remains constant, the change in effective stress in the reservoir is isotropic, and the stress path is horizontal in the *p'-q* plane. In other words, in a simplified 2D representation of the stress state, the Mohr circle would simply translate with no change in size (**Fig. 1a**). In the general case, however, fluid pressure reduction is accompanied by a reduction in the total horizontal stress, termed *field scale σ_h/p coupling* (Hillis, 2001), which leads to the development of deviatoric stresses and the associated expansion of the Mohr Coulomb circle (**Fig 1b**).

The total vertical stress is often assumed to be defined by the weight of the overburden and to remain unchanged during reservoir production. This ideal case, however, is not valid when stress arching occurs; i.e. when part of the overburden weight is transmitted to the sideburden during reservoir compaction (Khan et al, 2000; Sayers and Schutjens, 2007).

Estimating the stress evolution during reservoir production is important to predict phenomena such as the generation or reactivation of faults, pore collapse, bedding-parallel slip, casing deformation, or seismic activity among others (Sayers and Schutjens, 2007; Van Eijs et al. 2006, Verdon et al. 2010; Angus et al., in review). The stress state is also a key input in designing hydraulic fracture stimulation plans, as the stress state determines the injection fluid pressure necessary to fracture the rock as well as the fracture propagation direction. Furthermore, in geophysical studies, identification of relative change in the horizontal and vertical stresses is extremely beneficial, as a larger change in total horizontal stress than the accompanying change in vertical stress may lead to significant changes in elastic-wave anisotropy (Sayers 2006; Verdon et al., 2008).

Numerical and theoretical studies exist in the literature that analyze the controls of the reservoir geometry and the material properties on the reservoir stress path during production. A stiff overburden (compared to the reservoir stiffness) will promote stress arching as the reservoir compacts (Sayers and Schutjens, 2007), and stress changes will occur more in the overburden than within the reservoir (Alassi et al. 2006). Khan et al. (2000) and Sayers (2006) show that K tends towards the oedometric value as the aspect ratio of reservoir length to thickness increases for isotropic reservoir properties. These studies are, however, based on 2D or axisimmetric reservoir geometries (e.g. cylindrical or ellipsoidal).

This article analyzes the effect of 3D reservoir geometry on the reservoir stress path during production. A series of numerical studies are performed to predict the stress path parameters as a function of 3D reservoir geometry and for contrasts in elastic material properties in the reservoir and the bounding material. These results are valuable for prediction of the stress evolution during production, but, also, may be used to improve the accuracy of fluid flow simulations. This is achieved by introducing the influence of the stress path parameters in the pore volume multipliers tables used by standard production simulation modelling software packages (e.g. Eclipse[TM], Tempest[TM]), and thereby providing a more realistic spatial distribution of porosity change during production.

After this introduction, the stress path parameters will be defined in Section 2. The effect of reservoir geometry and material properties on the stress path is then studied in Section 3. Section 4 introduces the effect of the stress path parameters on fluid flow simulations. The paper finishes with the concluding remarks.

2. DEFINITION OF STRESS PATH PARAMETERS

The stress evolution during reservoir production depends mainly on the initial stress state prior to production, the material properties (both reservoir and bounding material) and the reservoir geometry, and can be defined in terms of the "*reservoir*

stress path parameters". In this definition it is assumed that the maximum and minimum principal stresses are vertical and horizontal respectively, i.e. uniaxial burial/extensional stress regime.

A pressure drop Δp is considered due to fluid withdrawal from a reservoir, which according to Terzaghi's generalized effective stress principle (Terzaghi, 1943; Biot and Willis, 1957) promotes a change of the effective and total stresses:

$$\Delta\sigma'_v = \Delta\sigma_v - \alpha\Delta p \qquad\qquad (1)$$
$$\Delta\sigma'_h = \Delta\sigma_h - \alpha\Delta p \qquad\qquad (2)$$

where $\Delta\sigma'_v$ and $\Delta\sigma'_h$ are the effective vertical and minimum horizontal stresses respectively, $\Delta\sigma_v$ and $\Delta\sigma_h$ are the total stress values, and α is the Biot's parameter (Biot and Willis, 1957). Usually, α is assumed to be equal to 1. However, in reality it may vary between 0 and 1 with typical values being between 0.3 and 1 (e.g. Fatt, 1959; Franquet and Abass, 1999).

Three "*stress path parameters*" are defined, which describe the evolution of the stress state in the reservoir during production:

$$\gamma_v = \frac{\Delta\sigma_v}{\Delta p} \qquad\qquad (3)$$

$$\gamma_h = \frac{\Delta\sigma_h}{\Delta p} \qquad\qquad (4)$$

$$K = \frac{\Delta\sigma'_h}{\Delta\sigma'_v} = \frac{\gamma_h - \alpha}{\gamma_v - \alpha} \qquad\qquad (5)$$

Here we refer to γ_v as the "*stress arching parameter*", γ_h as the "*horizontal stress path parameter*" and K as the "*deviatoric stress path parameter*". Parameter γ_h is usually estimated in the field with hydraulic fracturing tests (e.g. micro-frac or extended leak-off tests). Equation (5) shows that only two out of the three stress path parameters are independent. Parameters γ_v and K are chosen in this work as the reference parameters to study the stress path.

The parameter γ_v describes the amount of stress arching during production. If γ_v is high, stress arching occurs and the effective stress evolution is minimal in the reservoir and is mostly manifested in the overburden in the form of unloading (vertical stress decreases), and in the sideburden in the form of loading.

The parameter K describes the development of stress anisotropy. Lower values of K correspond to lower changes in horizontal effective stress than in vertical effective stress, or in other words, to an increase in stress anisotropy. However, stress anisotropy can only increase if the vertical effective stress increases, or more specifically providing stress arching does not occur (i.e. with low values γ_v).

In terms of a Mohr circle representation of the stress state, K defines the new size of the circle and γ_v defines the new right hand side coordinate of the circle. This is summarized in **Fig. 1**:

a) If $K \rightarrow 1$, the development of deviatoric stress is miminum and the Mohr circle tends to translate, giving:
1. circle a1 with little translation if stress arching occurs, i.e. $\gamma_v \rightarrow \alpha$;
2. circle a2 with large translation if stress arching does not occur, i.e. $\gamma_v \rightarrow 0$. This case is more prone to pore collapse.

b) If $K \rightarrow 0$, the development of deviatoric stress will be maximum, giving:
1. circle b1 with little growth if stress arching occurs, i.e. $\gamma_v \rightarrow \alpha$;
2. circle b2 with maximum growth if stress arching does not occur, i.e. $\gamma_v \rightarrow 0$. This case is more prone to shear failure, although that depends on the initial stress state and the material properties.
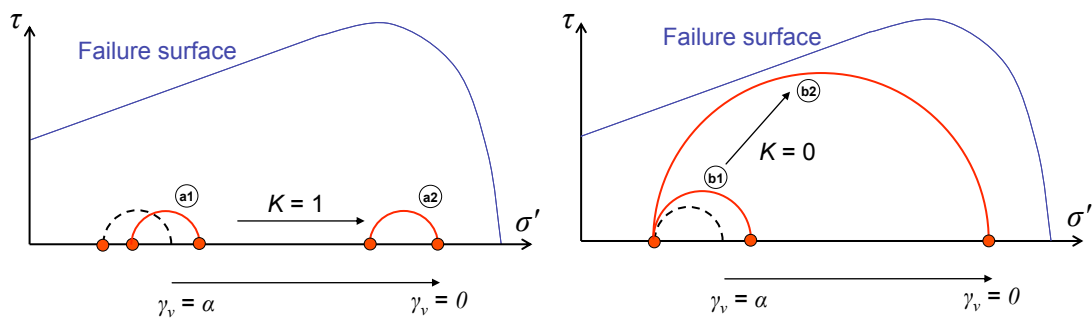
Figure 1. *Mohr circle evolution during reservoir depletion as a function of K and γ_v if (a) K = 1 or (b) K = 0.*

It should be noted that there is often a great deal of inconsistency between the use and definition of the stress path parameters in the reservoir engineering literature, so great care needs to be taken when collating data. Whereas some authors use K to denote the "stress path" (Khan et al. 2000; Sayers, 2006), others use γ_h (Santarelli et al. 1998; Goulty, 2003). Stress path results can refer to experimental studies or to field data obtained using hydrofracturing type tests, and also as in many situations it is assumed that $\gamma_v = 0$ (i.e. no stress arching effect), and in this case K and γ_h are equivalent (Equation 5).

As summarized by Goulty (2003), K is in the range of 0.4-0.6 during the normal compaction of chalk. K commonly has values around 0.3-0.4 for sands, 0.7 or greater for clays, and values between these extremes in silts (Jones, 1999). Hettema et al. (1998) analyzed a discrepancy between the stress path obtained from uniaxial compaction experiments ($\gamma_h = 0.8$) and the stress path inferred from the Groningen field data ($\gamma_h = 0.4$). A summary of measured stress path data from some producing petroleum reservoirs is presented in Table 1.

Reservoir	Lithology	γ_h	Reference
Waskom field	Sandstone (Travis Peak)	0.46	Holditch et al. (1987)
Several: West Texas	Sandstone (Vicksburg)	0.38-0.63	Salz (1977)

Unkown	Unfaulted poorly lithified sand (probably Mid-Jurassic)	0.7	Santarelli et al. (1998)
Unknown	Faulted poorly lithified sand	0.42	Santarelli et al. (1998)
Ekofisk	Chalk	0.8	Teufel et al. (1991)
Groningen	Lithfied sandstone (Rotliegend)	0.2-0.6	Hettema et al (1998)
Magnus	Lithified sandstone (Jurassic)	0.68	Shepherd (1991)
West Sole	Lithfied sandstone (Rotleiged)	1.18	Winter & King (1991)
Wytch farm	Triassic sandstone	0.65	Addis (1997)
Venture Field, Nova Scotia	Sandstone	0.56	Ervine & Bell (1987)

Table 1. Data on the horizontal stress path parameter γ_h as derived from the literature

In terms of controls on reservoir stress path, a commonly used simplification is that the rock response is poroelastic and deforms uniaxially during production (i.e. passive basin or oedometric). In this case, the parameter K is a function of the rock Poisson's ratio v:

$$K = \frac{v}{1-v} \qquad (6)$$

And if no stress arching is taking place ($\gamma_v = 0$):

$$\gamma_h = \alpha \frac{1-2v}{1-v} \qquad (7)$$

In faulted reservoirs, the stress path can be controlled by critically stressed faults and their (residual) friction angle (Addis et al. 1996, 1998, Wu et al.1998).

It has also been experimentally demonstrated for some fine-grained sediments that under oedometric conditions, and for overconsolidated materials, the stress path parameter K evolves from the elastic value in Equation 6 to an asymptotic value corresponding to the uniaxial plastic consolidation of the material (Pouya et al 1998).

3. EFFECT OF RESERVOIR GEOMETRY AND MATERIAL PROPERTIES ON RESERVOIR STRESS PATH

A series of 3D numerical coupled hydro-mechanical analyses is performed to study the effect of reservoir geometry and material properties on the development of stress arching and stress anisotropy during production. The values for the stress path parameters γ_v and K (Equations 3 and 5) are calculated numerically, and given as a function of reservoir aspect ratios and material properties.

The numerical analyses consider a pressure drop of 10 MPa within a reservoir located at 3048 m (10000 ft) depth. Ten reservoir geometries are analyzed (**Fig. 2**), which combine low, mid and high aspect ratios in the two vertical planes XZ and YZ, covering extreme cases like small, large and thin reservoirs, and all the intermediate shapes. A small reservoir (aspect ratio 5 in XZ and YZ) or a thin plank-type reservoir (aspect ratio 100 in XZ and 5 YZ) are analogues to highly compartmentalised reservoirs, and a large reservoir (aspect ratio 100 in XZ and YZ) can be associated to standard blanket-type reservoirs. The influence of the bounding and reservoir Young's modulus and Poisson's ratio on the stress path is studied for each geometry. The well is located in the centre of the reservoirs. The remaining material parameters and boundary conditions are fixed and correspond to a case study proposed by Dean et al. (2003).

case	X length : a (feet)	Y length : b (feet)	Z length (feet)
5x:5y:1z	1250	1250	250
10x:5y:1z	2500		
50x:5y:1z	12500		
100x:5y:1z	25000		
10x:10y:1z	2500	2500	
50x:10y:1z	12500		
100x:10y:1z	25000		
50x:50y:1z	12500	12500	
100x:50y:1z	25000		
100x:100y:1z	25000	25000	
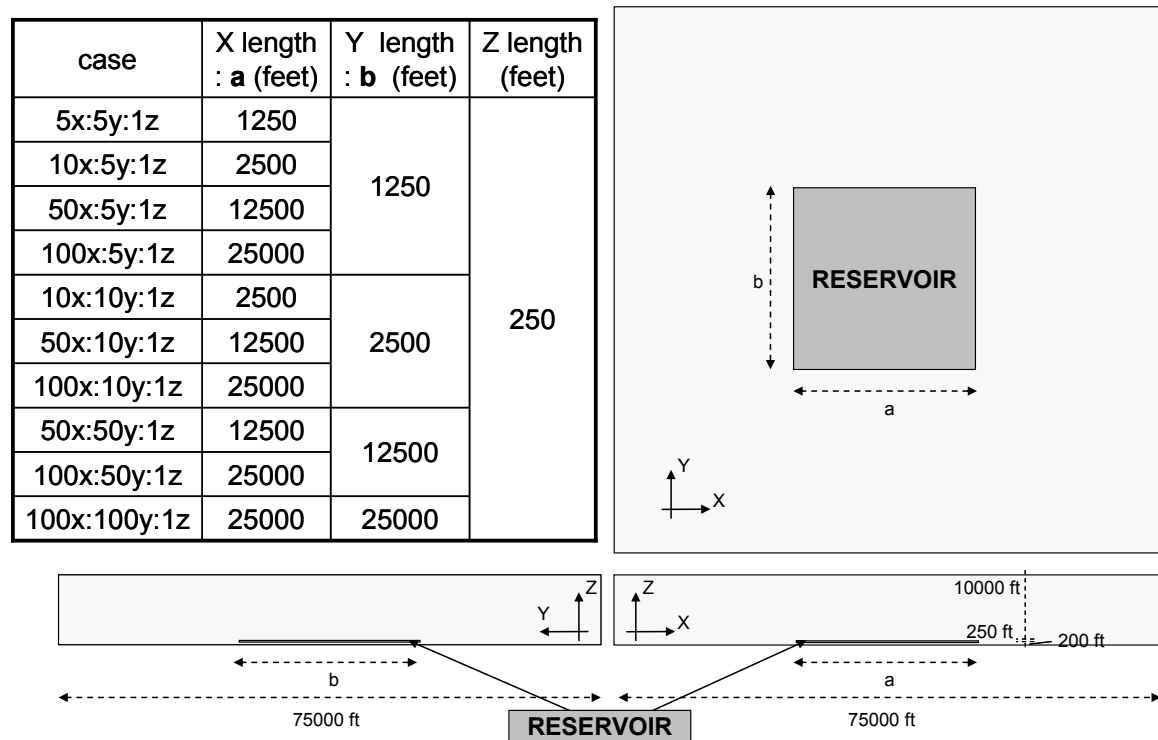
Figure 2 Reservoir geometries/dimensions analyzed.

The simulations are performed using a code that explicitly couples the TEMPEST production simulation model (Roxar Ltd.) for the flow calculations with ELFEN finite element program (Rockfield Software Ltd.) for the geomechanical simulations. An MPI interface developed by Rockfield Software Ltd. controls the transfer of fluid pressure data from TEMPEST to ELFEN, pore volume multiplier data from ELFEN to TEMPEST, and also at which time-steps it is necessary to make this information exchange (Crook and Dutko, 2006).

The results shown in this section extend to full 3D the 2D and axisymmetric studies existing in the literature (Khan and Teufel, 1996; Khan et al. 2000; Alassi et al. 2006; Sayers, 2006; Sayers and Schutjens, 2007), showing, when comparable, a good agreement with their results as explained next.

3.1 Influence of Young's Modulus on γ_v and K

Two groups of simulations are performed to study the effect of the reservoir and the bounding rock Young's moduli. The first group fixes the reservoir Young's modulus (E_r = 6.89 GPa) and analyzes the effect of varying the bounding material Young's modulus (E_b). The second group fixes E_b = 6.89 GPa and varies E_r. For a given geometry and for a given ratio E_r/E_b, the results, in terms of stress path parameters, are very similar regardless of the absolute value of the moduli (average difference lower than 1%). The numerical results, therefore, are presented in terms of the ratio E_r/E_b.

Fig. 3 provides the values of γ_v and K in the well zone as a function of the ratio E_r/E_b and the reservoir geometry. The axes in **Fig. 3** represent:

- x: aspect ratio in the X direction (i.e. reservoir length in X over thickness in Z; e.g. 50 for a reservoir that is 50 times longer in X than thick in Z)
- y: aspect ratio in the Y direction
- z: stress path parameter value for the geometry with aspect ratios (x,y)

Fig. 3a shows that γ_v is very low if the reservoir is 10 times stiffer than the bounding material (E_r/E_b = 10), and there is negligible stress arching for all geometries. As the reservoir stiffness is decreased, γ_v increases, especially for reservoirs with low aspect ratios in either one or both directions. γ_v values are close to one when the reservoir is much softer (E_r/E_b = 0.01) and is either small or plank-like (i.e. small aspect ratios in X or/and in Y); in these type of reservoirs, stress arching is significant and the weight of the overburden is partly supported by the sideburden.

Fig. 3b shows that for a contrast E_r/E_b = 10, K is high for small reservoirs and tends to decrease towards the oedometric value as one or the two horizontal dimensions of the reservoir increases. The effect of reservoir geometry on K is not as pronounced as for γ_v, and the oedometric hypothesis seems a good approximation unless the reservoir is small and the contrast in elastic properties is large.
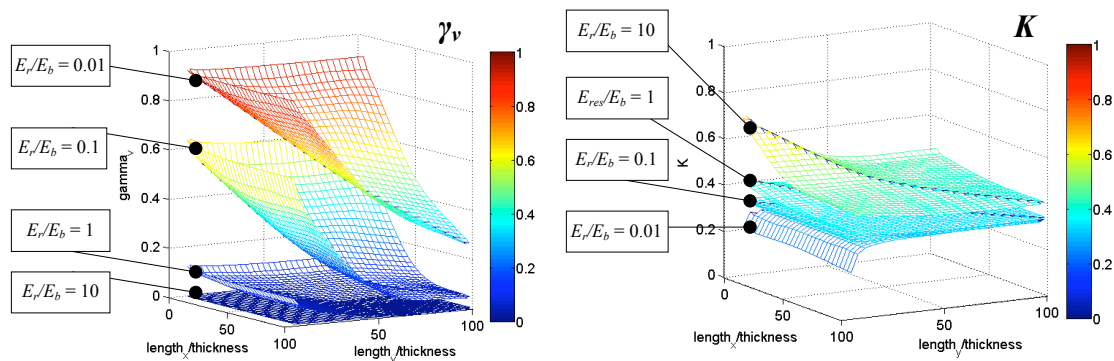
Figure 3. Parameters (a) γ_v and (b) K as a function of reservoir geometry and E_r/E_b

Similar plots to **Fig. 3** have been produced for other areas of the reservoir (not shown), and average values for a reservoir may be calculated. The stress parameter evolution in the well area, however, is usually the most critical and is the most useful when predicting well failure and for hydraulic fracturing design.

3.2 Influence of Poisson's ratio on γ_v and K

Fig. 4 provides the stress path parameters γ_v (**Fig. 4a**) and K (**Fig. 4b**) in the well zone as a function of the reservoir geometry and reservoir Poisson's ratio, for which four values have been considered ($v_r = 0.15; 0.25; 0.35; 0.49$). In this group of simulations a Young's modulus of 6.89 GPa has been used for the reservoir and bounding material; the bounding material Poisson's ratio is $v_b = 0.25$.

Fig. 4a shows that the value of v_r does not significantly alter the parameter γ_v for the studied ratio $E_r/E_b=1$. It is clear, however, that increasing v_r reduces stress arching because the reservoir is less compressible. On the other hand, K is significantly influenced by v_r and it tends to the uniaxial compaction value (Eq. 6) independently of the geometry as v_r increases. Small reservoirs exhibit higher K than the uniaxial compaction value if v_r is small.

Simulations have also been performed with a fixed value of the reservoir Poisson's ratio ($v_r = 0.25$), and for three values of the bounding material Poisson's ratio ($v_b = 0.125; 0.25; 0.49$). The influence of v_b in the stress path parameters is very small for the studied ratio $E_r/E_b=1$, obtaining almost identical surfaces regardless of v_b as shown in **Fig. 5a** and **Fig. 5b**.
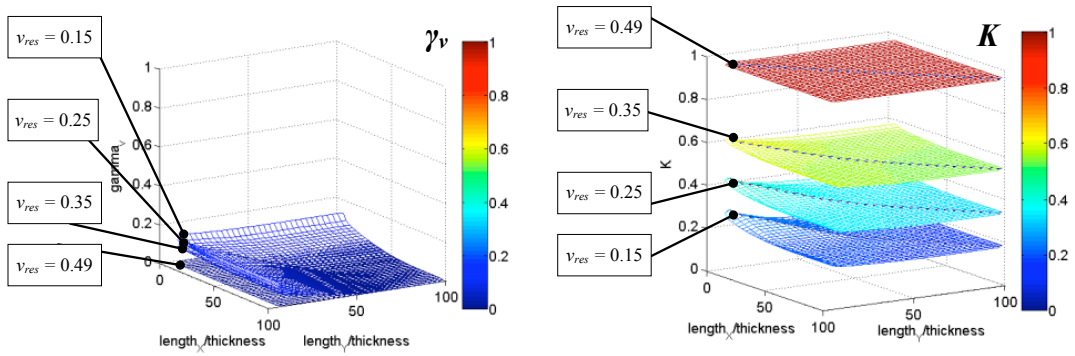
Figure 4. Parameters (a) γ_v and (b) K as a function of reservoir geometry and v_r
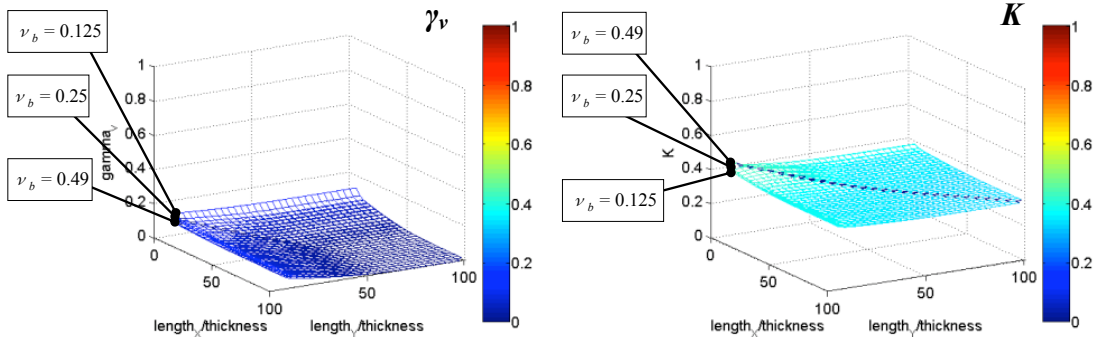
Figure 5. Parameters (a) γ_v and (b) K as a function of reservoir geometry and v_b

Vertical sections of the surfaces in **Fig. 3**, **Fig. 4** and **Fig. 5** along the line $x = y$ give curves that compare well with the 2D and axisymmetric results existing in the

literature (Khan and Teufel, 1996; Khan et al. 2000; Alassi et al. 2006; Sayers (2006); Sayers and Schutjens, 2007).

4. IMPROVING FLUID FLOW SIMULATIONS BASED ON THE STRESS PATH PARAMETERS

In fluid flow numerical simulations of reservoir production, the effect of the reservoir compaction is introduced via pore volume multiplier tables that are often based on oedometric test results. This section studies the accuracy of non-coupled simulations based on these assumptions compared to coupled fluid flow-geomechanical models, and the improvement in accuracy obtained if the effect of the stress path parameters are introduced in the pore volume multiplier tables in non-coupled simulations.

Reservoir production is solved using a coupled HM code and a standalone fluid flow simulator. The comparison between both solutions is made in terms of the hydrocarbon average pore pressure. The coupled simulation is performed using the same explicit coupling scheme between TEMPEST and ELFEN used in Section 2 (Crook and Dutko, 2006). The non-coupled simulation is run using the TEMPEST production simulator only. The look-up table of pore volume multipliers (PVM) against pressure for the fluid flow simulation is obtained by conducting a numerical consolidation test. An elasto-plastic model with non-linear elasticity is used in these simulations unlike the idealized linear elastic model adopted in previous section.

4.1 Geometry and materials

A large blanket-type reservoir (dimensions 100x:100y:1z in **Fig. 2**) is used for the sake of generalization. A soft material that undergoes large amounts of pore collapse during production is considered for the reservoir, so moderate stress arching is expected to occur in this case.

The constitutive model used for the reservoir is a critical state-based model specially developed for soft rocks (Crook et al. 2002), which simulates the pore collapse that sometimes occurs during reservoir production. A Cam-Clay type expression is considered for the definition of the elasticity:

$$K = K_0 + \frac{1}{\kappa}\left(\frac{1}{1-\phi}\right)\sigma'_m \qquad (8)$$

where K is the bulk modulus, κ a model parameter, ϕ the porosity and σ'_m the effective mean stress.

The initial Young's modulus (before starting production) is approximately $E = 6.8$ GPa. The Poisson's ratio is $v = 0.2$.

The bounding material is considered elastic with a depth variable Young's modulus according to Equation 8, with $K_0 = 1000$ MPa and $\kappa = 0.01$. The resulting Young's modulus ranges from approximately 2GPa at the surface (0m depth) to 6.8GPa at the bottom of the model. The Poisson's ratio is $v = 0.2$.

4.2 Generation of the PVM tables

A numerical compaction simulation is performed to obtain the PVM table that will be introduced into the flow simulator input data for the uncoupled simulation. **Fig. 6** shows a schematic of the boundary, initial and loading conditions. The specimen is loaded by an upper distributed load and is assigned an initial pore pressure, both corresponding to the average reservoir in-situ conditions. The specimen is laterally constrained on the vertical boundaries and fully constrained at the bottom. The pore pressure is linearly reduced (**Fig. 6)**, which increases the effective stresses acting on the specimen and induces compaction of the reservoir rock in a similar manner to a standard compaction test, where the applied vertical load is increased under drained conditions.

The compaction simulation has two main assumptions, both of which are commonly adopted in practical reservoir engineering:

- the material deforms uniaxially (vertical compaction only),
- the total vertical stress acting on the material does not change during reservoir production (no stress arching).
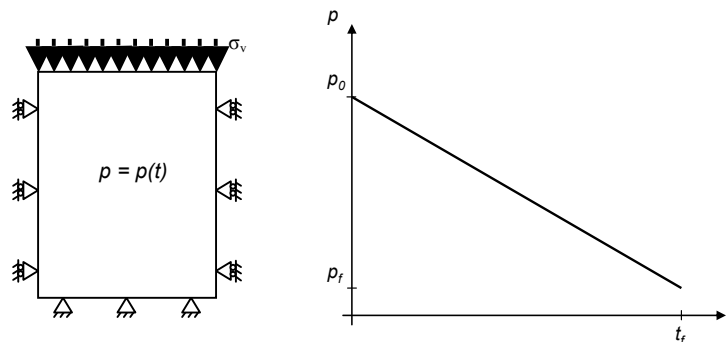
Figure 6. Boundary conditions and pore pressure drawdown during the numerical compaction simulation.

4.3 Coupled and non-coupled results.

The results are presented for a large reservoir where the ratio of horizontal extension to reservoir thickness is high, which is representative of the majority of field cases. The procedure is, however, equally valid for small and thin reservoirs, which are more prone to show stress arching for a large range of reservoir material stiffness as explained in Section 2, and also to deviate from uniaxial deformation.

Fig.7a shows the stress and yield surface evolution during the material compaction test, and **Fig. 7b** plots the PVM table resulting from the experiment. Note that the material is normally consolidated and plastic compaction is occurring from the onset of the experiment. For this reason, the elastic results shown in Section 3 are not directly applicable.
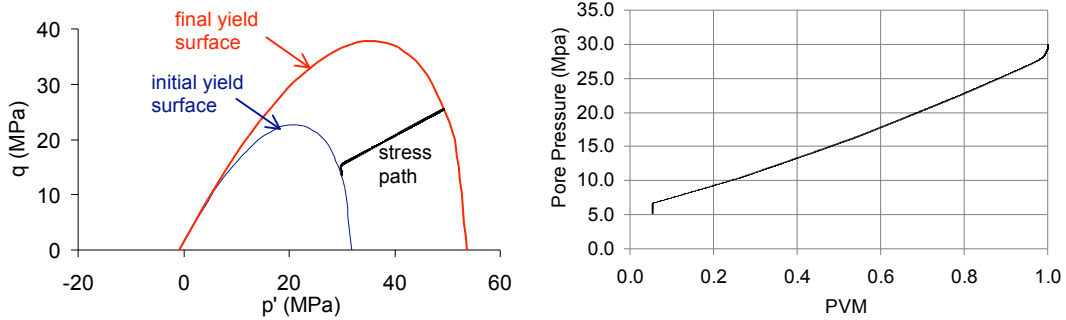
Figure7. Numerical compaction test results: (a) stress path in p'q plane (b) PVM table

Fig. 8a compares the coupled results with the non-coupled predictions conditioned using a constant PVM table for the reservoir. The non-coupled simulation overestimates the pore pressure relative to the coupled prediction. The main reason for this difference is that production from a very soft reservoir (compared to the bounding material) causes stress arching, which reduces the vertical total stress acting on the reservoir and the pore pressure support provided by compaction drive. Stress arching and the associated reduction in pore pressure support are captured by the coupled model, but the uncoupled simulation overestimates the compaction driven pore pressure.

(a)   (b)
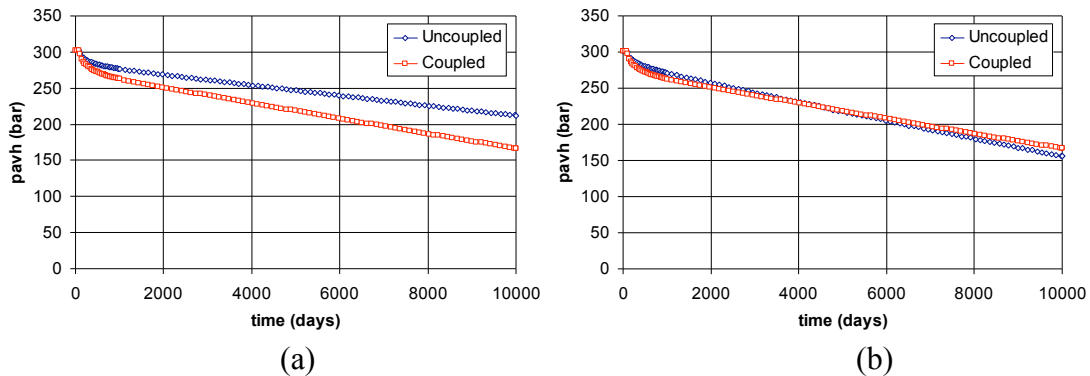
Figure 8. Coupled vs non-coupled solutions (a) PVM table without stress arching effect (b) PVM table with average stress arching effect

The PVM table can, however, be adapted to account for the stress arching and the associated decrease in total vertical load acting on the reservoir. According to the coupled results, the stress arching parameter γ_v is, on average, 0.4. The numerical compaction test is repeated with an upper vertical load that linearly reduces during pore pressure drawdown according to γ_v=0.4 as shown in **Fig.9**. Since the vertical stress reduces during pore pressure drawdown, the rock compacts less, obtaining the new PVM table shown in **Fig. 10b**, which incorporates the average effect of stress arching.
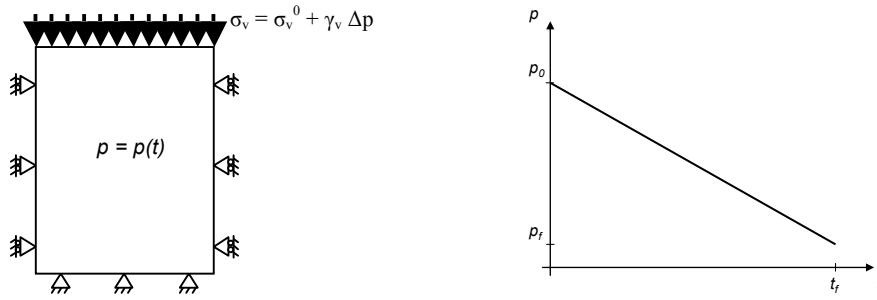
Figure 9. Modified boundary conditions and pore pressure drawdown during the modified numerical compaction simulation.
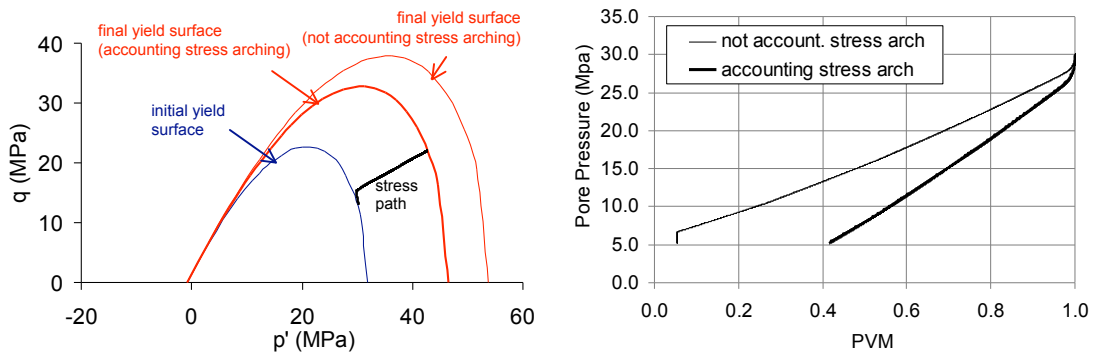
Figure 10. Numerical compaction test results accounting for stress arching: (a) stress path in p'q plane (b) PVM table.

The new PVM table that introduces the effect of stress arching improves the uncoupled results, producing an average pore pressure drawdown much closer to the coupled pore pressure profile as shown in **Fig. 8b**.

The stress arching effect is not homogeneous throughout the reservoir, and, for example, it can be stronger at the boundaries of the reservoir, and depend on the location of the well and the materials. A more realistic uncoupled approach would be to divide the reservoir in sectors according to the distribution of stress arching, quantified by γ_v, and use different PVM tables accordingly.

The PVM tables may also be improved by using a more general lateral boundary condition in the numerical compaction test, with a prescribed horizontal stress that linearly varies with pore pressure drawdown according to γ_h. Care should be taken, however, with the evolution of the out-of-plane horizontal stress.

The stress path parameters can be obtained based on look-up tables similar to those presented in Section 3 of this article, which provide the parameters suitable for a specific geometry and set of materials. If these are not available, a preliminary HM coupled analysis may be used to locate areas that deviate from standard non-stress arching and uni-dimensional compactional behaviour, and therefore enable redefinition of the PVM tables for these regions based on the modified 1D compaction tests. This approach is suitable to improve fluid flow simulations in reservoirs with intermediate complexity. A more general approach is the use of spatially varying PVM tables for the stand-alone reservoir simulation that are

computed directly from coupled simulations (Pettersen, 2008; Pettersen and Kristiansen, 2009).

5. CONCLUDING REMARKS

Key controls on reservoir stress path during production including 3D reservoir geometry and contrast in elastic properties between the reservoir and the bounding material have been analyzed. The reservoir stress path is defined in terms of the stress arching parameter, γ_v, that quantifies the amount of stress arching occurring during reservoir production, and the deviatoric stress path parameter, K, which quantifies the amount of stress anisotropy developed during production. For the range of material properties analyzed, the stress path parameters depend on the Young's modulus contrast between the reservoir and the bounding material independently of the Young's moduli absolute values. Stress anisotropy reduces with the bounding material Young's modulus, especially for small reservoirs, but as the reservoir extends in one or the two horizontal directions, K tends to the oedometric value governed by the reservoir Poisson's ratio. Special attention is paid to the stress arching effect, which is important in small or thin reservoirs that are soft compared to the bounding material. Stiff reservoirs do not show stress arching independently of the geometry. A methodology is presented to improve non-coupled simulations by introducing the effect of the stress path parameters in the look-up tables of pore volume multipliers.

REFERENCES

Addis MA, Last NC, Yassir NA (1996) Estimation of horizontal stresses at depth in faulted regions and their relationship to pore pressure variations. SPE Formation Evaluation 11(1), 11-18

Addis MA (1997) The Stress-Depletion Response Of Reservoirs, SPE 38720-MS; SPE Annual Technical Conference and Exhibition, San Antonio, Texas

Addis MA, Choi X, Gunning J (1998) The influence of the reservoir stress-depletion response on the lifetime considerations of well completion design. SPE/ISRM 47289; SPE/ISRM Rock Mechanics in Petroleum Engineering, 8-10 July 1998, Trondheim, Norway.

Alassi HTI, Liming L, Holt RM (2006) Discrete element modeling of stress and strain evolution within and outside a depleting reservoir, *Pure and Applied Geophysics*, 163: 1131-1151.

Angus, DA Kendall, JM, Skachkov, S, Fisher, QJ, Dutko, M, Crook, AJL (in review) Predicting microseismicity from coupled fluid-flow and geomechanical simulation: A tool for identifying reservoir compartmentalisation, Geophysical Prospecting.

Biot MA, Willis DG (1957) The elastic coefficients of the theory of consolidation, *ASME Journal of Applied Mechanics*, 24: 594-601.

Crook T, Dutko M (2006) IPEGG (Integrated Petroleum Engineering Geophysics and Geomechanics) More/ELFEN Coupling. *Internal report number PFS/1716, Rockfield Software Limited*, Swansea, UK.

Crook AJL, Yu J-G, Willson SM (2002) Development of an orthotropic 3D elastoplastic material model for shale. *Society of Petroleum Engineers* paper 78238.

Dean RH, Gai X, Stone CM, Minkoff SE (2003) A comparison of techniques for coupling porous flow and geomechanics, *Society of Petroleum Engineers* paper 79709; presented at the 2003 SPE Reservoir Simulation Symposium, Houston, Texas, USA.

Ervine WB, Bell JS (1987) Subsurface in situ stress magnitudes from oil well drilling records: an example from the Venture area, offshore Eastern Canada, *Canad. J. Earth Sci.*, 24: 1748-1759

Fatt I (1959) The Biot-Willis elastic coefficients for a sandstone, *Journal of Applied Mechanics*, 26: 296-297

Franquet JA, Abass HH (1999) Experimental evaluation of Biot's poroelastic parameter - Three different methods, in *37th U.S. Symposium on Rock Mechanics (USRMS)*, June 7-9 Vail, CO, Balkema, Rotterdam

Goulty NR (2003) Reservoir stress path during depletion of Norwegian chalk oilfields, *Petroleum Geoscience*, 9: 233-241.

Hettema MHH, Schutjens PMTM, Verboom BJM, Gussinklo HJ (1998) Production-induced compaction of sandstone reservoirs: the strong influence of field stress, *Society of Petroleum Engineers* paper 50630, presented at the 1998 SPE European Conference, The Hague, The Netherlands.

Hillis RR (2001) Coupled changes in pore pressure and stress in oil fields and sedimentary basins, *Petroleum Geoscience*, 7: 419-425

Holditch SA, Robinson BM, Whitehead WS (1987) The Analysis of Complex Travis Peak Reservoirs in East Texas, *Society of Petroleum Engineers* paper 16427; presented at the 1987 Low Permeability Reservoir Symposium, Denver, CO.

Jones ME (1994) Mechanical principles of sediment deformation. In *The Geological Deformation of Sediments*; Maltman, A. (ed.). Chapman & Hall, London, pp 37–71.

Khan M., Teufel LW, Zheng Z (2000) Determining the effect of geological and geomechanical parameters on reservoir stress path through numerical simulation, *Society of Petroleum Engineers* paper 63261, presented at the 2000 SPE Annual Technical Conference and Exhibition, Dallas, Texas, USA.

Pettersen Ø (2008) Using relations between stress and fluid pressure for improved compaction modelling in flow simulation and increased efficiency in coupled rock mechanics simulation, *Petroleum Geoscience*, 14(4): 399-409

Pettersen Ø, Kristiansen TG (2009) Improved compaction modeling in reservoir simulation and coupled rock mechanics/flow simulation, with examples from the Valhall Field, *SPE Reservoir Evaluation & Engineering*, 12(2): 329-340

Pouya A, Djéran-Maigre I, Lamoureux-Var V, Grunberger D (1998) Mechanical behaviour of fine grained sediments: experimental compaction and three-dimensional constitutive model, Marine and Petroleum Geology, 15: 129-143.

Salz LB (1977) Relationship between fracture propagation pressure and pore pressure, *Society of Petroleum Engineers* paper 6870, in SPE Annual Fall Technical Conference and Exhibition, Denver, Colorado, 7p

Santarelli FJ, Tronvoli JT, Svennekjaer M, Skeie H, Henriksen R, Bratli RK (1998) Reservoir stress path: the depletion and the rebound, *Society of Petroleum Engineers/International Society of Rock Mechanics* paper 47350, presented at the SPRE/ISRM Eurock'98 held in Trondheim, Norway.

Sayers CM (2006) Sensitivity of time-lapse seismic to reservoir stress path, *Geophysical Prospecting*, 24: 369-380.

Sayers CM, Schutjens MTM (2007) An introduction to reservoir geomechanics, *The Leading Edge*, May 2007: 597-601.

Sheperd M (1991) The Magnus Field, Blocks 211/7a, 12a, UK North Sea. In Abbotts, I.L. (ed.) United Kingdom Oil and Gas Fields, 25 Years Commemorative Volume. Geological Society, London, Memoir 14, 153-157

Terzaghi K (1943) *Theoretical Soil Mechanics*, John Wiley and Sons, New York

Teufel LW, Rhett DW, Farrell HP (1991) Effect of reservoir depletion and pore pressure drawndown on in situ stress and deformation in the Ekofisk field, North Sea. In *Rock mechanics as a Multidisciplinary Science*, ed. JC Roegiers, Balkema, Rotterdam: 63-72.

Van Eijs RMHE, Mulders FMM, Nepveu M, Kenter CJ, Scheffers BC (2006) Correlation between hydrocarbon reservoir properties and induced seismicity in the Netherlands, *Engineering Geology*, 84: 99-111.

Verdon, JP, Angus, DA, Kendall, JM, Hall, SA (2008) The effect of microstructure and nonlinear stress on anisotropic seismic velocities, Geophysics, 73(4), 206-216.

Verdon, JP, Kendall, JM, White, DJ, Angus, DA, Fisher, QJ, Urbancic, T (2010) Passive seismic monitoring of carbon dioxide storage at Weyburn, The Leading Edge, 29(2), 200-206.

Winter DA, King B (1991) The West Sole Field, Block 48/6, UK North Sea. In Abbotts, I.L. (ed.) United Kingdom Oil and Gas Fields, 25 Years Commemorative Volume. Geological Society, London, Memoir 14, 517-523.

Wu B, Addis MA, Last NC (1998) Stress Estimation in Faulted Regions: The Effect of Residual Friction, SPE-ISRM 47210; SPE/ISRM Eurock '98, Trondhelm, Norway